

3-D Medical Image Interpolation via Multi-Resolution Directional Correspondence*

WANG Lingfeng¹, YU Zeyun² and PAN Chunhong¹

(1.*Institute of Automation, Chinese Academy of Sciences, Beijing 100190, China*)

(2.*The Department of Computer Science, University of Wisconsin-Milwaukee, USA*)

Abstract — In this paper, we present a novel 3-D image interpolation method with high-quality feature preservation and low computational cost. The optimal direction of each voxel on the slices to be inserted is found by minimizing the smoothed directional correspondence using the Markov random field optimization approach. A multi-resolution scheme is employed to further reduce the memory consumption and computational costs as well as improve the interpolation accuracy. Extensive experiments are performed on medical image slices to evaluate the proposed approach, showing significant improvements in both accuracy and efficiency, as compared with the traditional interpolation techniques.

Key words — 3-D image interpolation, Markov random field, Multi-resolution.

I. Introduction

Many of the 3-D volumes are given by a sequence of 2-D image slices. Quite often, the in-plane resolutions, namely the resolutions in the x -and y -axes, are significantly higher than that in the z -axis. Therefore, it is important to insert some new images between the original slices to compensate the lost resolution in the z -axis. This problem is commonly known as 3-D image interpolation and will be the main target of the present paper.

In this work, to achieve a high-quality gray-scale interpolation with modest computational costs, a novel interpolation is proposed based on the directional correspondence. The principle of the present method is to determine the optimal directional correspondence of each voxel in missing slices. The voxels are described by the improved rotation-invariant gray-scale template, which is of low computational complexity as well as nice feature description. The optimal direction of each voxel is calculated by minimizing the smooth directional correspondence with the multi-resolution Markov random field optimization approach. With this novel approach, we are able to achieve two goals: preserving sharp and faithful features in the interpolated slices and keeping the computational cost affordable.

II. Previous Works

3-D image interpolation techniques can be mainly classified into two groups^[1], *i.e.*, the scene-based and object-based methods. In the scene-based methods, the intensity value is determined directly from the given image slices using such techniques as the linear and spline-based interpolation. In practice, the scene-based methods may result in very poor approximation with either noticeable artifacts or blurred features. Over the years, many object-based approaches, including morphology-based, shape-based, and registration-based, have been proposed to overcome the above drawbacks. The morphology-based methods^[2–4] explicitly handle the topology changes between consecutive slices by performing one-to-one, one-to-many, and zero-to-one correspondences iteratively. However, the input gray-scale slices must be pre-segmented into binary images. Shape information has been widely used in medical image interpolation for its ability of describing objects geometrically, and these methods are called shape-based methods^[5]. In Ref.[5], an n -D image slice is first lifted to a surface representation in the $(n+1)$ -D space, and then the binary shape-based method is applied on the $(n+1)$ -D binary image slice. The main limitation is its high computational costs due to the distance transform in higher dimensions. Recently, the registration-based methods^[6–9] are proposed to improve the interpolation quality. In Ref.[8], the missing slices are interpolated along the smooth and most coherent direction between consecutive slices instead of the z -axis. However, imprecise direction calculations may occur due to the rough hypothesis of 3-D unit vector of each cube.

III. Directional Correspondence Interpolation (DCI)

Suppose we are given a set of slices C_1, C_2, \dots, C_n of an object at z_1, z_2, \dots, z_n . The goal of the interpolation is to insert new slices $\hat{C}_1, \hat{C}_2, \dots, \hat{C}_n$ at $\hat{z}_1, \hat{z}_2, \dots, \hat{z}_n$. The overview of our algorithm is illustrated in Fig.1. Each interpolated slice is first analyzed by calculating the direction. Then, the intensity value is linear interpolated by two neighboring known

*Manuscript Received Jan. 2010; Accepted Nov. 2011. This work is supported by the National Basic Research Program of China (973 Program) (No.2012CB316304) and the National Natural Science Foundation of China (No.61175025, No.61005036, No.60975037).

slices along the direction. Thus, this problem can be simplified into a direction calculation problem.

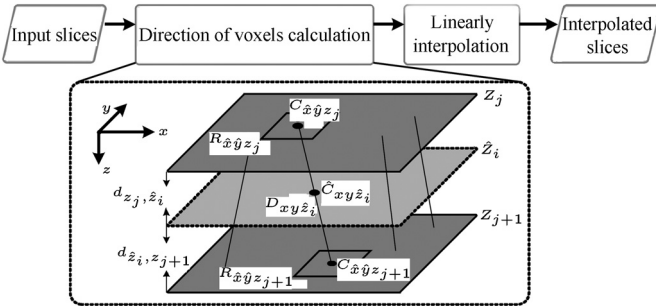


Fig. 1. An overview of DCI. D_{xyz_i} is the direction of \hat{C}_{xyz_i} . Voxel \hat{C}_{xyz_i} is linearly interpolated by $C_{\hat{x}\hat{y}z_j}$ and $C_{\hat{x}\hat{y}z_{j+1}}$

1. Single resolution Directional correspondence interpolation (SR-DCI)

The core of SR-DCI method is based on the Single resolution Direction calculation (SR-DC), which is further composed by three sub steps, *i.e.*, local feature extraction, direction calculation, and Single resolution Markov random field (SR-MRF) optimization^[10].

Local feature extraction The local feature R_{xyz_j} is described with a rotation-invariant grayscale template. We first calculate the gradient magnitude H and orientation θ of C , given by $H_{xy} = \sqrt{C_x^2 + C_y^2}$, $O_{xy} = \tan^{-1}(C_y/C_x)$, where C_x and C_y are the x -and y -gradients. Then, the local gradient orientation O_{xy} is calculated by $O_{xy} = \sum_{\dot{x}, \dot{y} \in N(x, y)} H_{\dot{x}\dot{y}} \theta_{\dot{x}\dot{y}}$, where x, y are the neighborhoods of x, y , that is, $\dot{x}, \dot{y} \in N(x, y)$. The neighborhood size is set 3×3 . Finally, a small local region o along O_{xy} is extracted as the local feature R_{xy} . The size of local region is set 7×7 .

Direction calculation All possible directions are given from a label set $L = \{l_0, l_1, l_2, \dots, l_m\}$. The direction calculation becomes label selection problem: for each voxel C_{xyz_i} , select a label l_k from the label set L so that the direction $D_{xyz_i} = l_k$, where $l_k \in L$.

To select the direction label l_k from L , we use the difference of two local features along the direction l_k as the cost of choosing l_k , as illustrated in Fig.1:

$$\begin{aligned} E_{x,y}(l_k) &= E(D_{xyz_i}) \\ &= \|R_{\hat{x}\hat{y}z_j} - R_{\hat{x}\hat{y}z_{j+1}}\| \\ &= \sum_{m,n=-3}^3 (C_{(\hat{x}+m)(\hat{y}+n)z_j} - C_{(\check{x}+m)(\check{y}+n)z_{j+1}})^2 \end{aligned} \quad (1)$$

where \hat{x}, \hat{y} and \check{x}, \check{y} are the corresponding x, y coordinates of the input slices at z_j and z_{j+1} , respectively. $R_{\hat{x}\hat{y}z_j}$ is the local feature at \hat{x}, \hat{y} of the input slice at z_{j+1} , while $R_{\hat{x}\hat{y}z_{j+1}}$ is the local feature at \check{x}, \check{y} of the input slice at z_{j+1} . To guarantee coherent spatial changes of direction, we restrict the adjacent voxels must have similar directions, given by

$$S_{x,y}(l_k, \tilde{l}_k) = S(D_{xyz_i}, D_{\hat{x}\hat{y}z_i}) = \varphi/\pi \quad (2)$$

where $\varphi \in [0, \pi]$ is the angle between l_k and \tilde{l}_k . By taking the smoothness constraint into consideration, the direction label

selection becomes the following optimization process:

$$\begin{aligned} D = \arg \min_D & \sum_{x,y} (E(D_{xyz_i}) \\ & + \lambda \sum_{C_{\hat{x}\hat{y}z_i} \in N(C_{xyz_i})} S(D_{xyz_i}, D_{\hat{x}\hat{y}z_i})) \end{aligned} \quad (3)$$

where λ is the user-provided weighting parameter. The weighting parameter λ is used to balance between the differences (see Eq.(1)) and the smoothness (see Eq.(2)). For example, a larger λ will result in that the directions in a local region are more similar with each other (or more smooth), but the differences along directions will be increased. When implementation, a small λ , *i.e.*, $\lambda = 1$, is experimentally employed to achieve the goal of balance.

SR-MRF The SR-MRF optimization is used to solve the Eq.(3) based on the simple loopy belief propagation method. Four-connected image grid graph is used as the spatial neighborhood. The more information about SR-MRF is presented in Algorithm 1 in detail.

Algorithm 1 SR-MRF Algorithm.

```

Data: Two adjacent slices  $C_{z_j}$  and  $C_{z_{j+1}}$ ; label set  $\mathcal{L}$ ;
weight constant  $\lambda$ ; iteration number  $n_i$ .
Result: Direction  $D$ .
1 Calculating  $E_{x,y}(l_k)$  based on Eq.(1); Calculating  $S_{x,y}(l_k, \tilde{l}_k)$ 
based on Eq.(2);
2 for each position  $x, y$  and each direction  $l_k$  in  $\mathcal{L}$  do
3    $IM_{x,y}(l_k) = 0$ ;  $rM_{x,y}(l_k) = 0$ ;  $uM_{x,y}(l_k) = 0$ ;
    $dM_{x,y}(l_k) = 0$ ;
4    $IM_{x,y}(l_k) = 0$ ;  $rML_{x,y}(l_k) = 0$ ;  $uML_{x,y}(l_k) = 0$ ;
    $dML_{x,y}(l_k) = 0$ ;
5   end
6   for  $i = 1$  to  $n$ ; do
7      $IML = IM$ ;  $rML = rM$ ;  $uML = uM$ ;  $dML = dM$ ;
8   for each position  $x, y$  and each direction  $l_k$  in  $\mathcal{L}$  do
9     for each direction  $\tilde{l}_k$  in  $\mathcal{L}$  do
10       $IMT(\tilde{l}_k) = E_{x,y}(l_k) + IM_{x,y}(\tilde{l}_k) + uML_{x,y}(\tilde{l}_k) +
          dML_{x,y}(\tilde{l}_k) + \lambda S_{x,y}(l_k, \tilde{l}_k)$ ;
11       $rMT(\tilde{l}_k) = E_{x,y}(l_k) + rML_{x,y}(\tilde{l}_k) + uML_{x,y}(\tilde{l}_k) +
          dML_{x,y}(\tilde{l}_k) + \lambda S_{x,y}(l_k, \tilde{l}_k)$ ;
12       $uMT(\tilde{l}_k) = E_{x,y}(l_k) + IML_{x,y}(\tilde{l}_k) + rML_{x,y}(\tilde{l}_k) +
          dML_{x,y}(\tilde{l}_k) + \lambda S_{x,y}(l_k, \tilde{l}_k)$ ;
13       $dMT(\tilde{l}_k) = E_{x,y}(l_k) + IML_{x,y}(\tilde{l}_k) + rML_{x,y}(\tilde{l}_k) +
          uML_{x,y}(\tilde{l}_k) + \lambda S_{x,y}(l_k, \tilde{l}_k)$ ;
14    end
15     $IM_{x,y}(l_k) = \min\{IMT\}$ ;  $rM_{x,y}(l_k) = \min\{rMT\}$ ;
       $uM_{x,y}(l_k) = \min\{uMT\}$ ;  $dM_{x,y}(l_k) = \min\{dMT\}$ ;
16  end
17 end
18 for each position  $x, y$  do
19   for each direction  $l_k$  in  $\mathcal{L}$  do
20      $mT(l_k) = E_{x,y}(l_k) + IM_{x,y}(\tilde{l}_k) + rM_{x,y}(\tilde{l}_k) +
          uM_{x,y}(\tilde{l}_k) + dM_{x,y}(\tilde{l}_k) + \lambda S_{x,y}(l_k, \tilde{l}_k)$ ;
21   end
22    $D_{x,y} = \text{obtaining direction } l, \text{ which satisfies that }$ 
    $mT(l) \leq mT(l_k) \text{ for all } l_k \in \mathcal{L}$ .
23 end

```

2. Multi resolution Directional correspondence interpolation (MR-DCI)

In MR-DCI, the coarse direction is first calculated in the low-resolution slices, and then refined in the high-resolution slices. A Gaussian pyramid G is constructed for each input slice C , given by $G^i = \downarrow 2[G^{i-1} \otimes g]$ (G^i denotes the i -th level),

where $\downarrow 2[]$ is the $2 \times$ down-sampling operation, g is the Gaussian kernel, and $G^0 = C$. For each G^i , the corresponding direction field is denoted as D^i . Then, we perform the SR-DC module iteratively to calculate the direction field D^i of high-level by using the i -th level slices G^i and last low-level direction field D^{i+1} until the largest level slice's direction field $D = D^0$ is reached. In the refinement step, the high-level direction field is first initialized by up-sampling operation on low-level direction field D^{i+1} , $\bar{D}^i = \uparrow 2[D^{i+1}]$, where $\uparrow 2[]$ is the $2 \times$ up-sampling operation. Then, it is refined by $D^i = \bar{D}^i + \Delta D^i$, where

$$\begin{aligned} \Delta D^i = & \arg \min_{\Delta D^i} \sum_{x,y} \left(E(\bar{D}_{xy}^i + \Delta D_{xy}^i) \right. \\ & \left. + \lambda \sum_{G_{\hat{x}\hat{y}}^i \in (NG_{\hat{x}\hat{y}}^i)} S(\bar{D}_{xy}^i + \Delta D_{xy}^i, \bar{D}_{\hat{x}\hat{y}}^i + \Delta D_{\hat{x}\hat{y}}^i) \right) \end{aligned} \quad (4)$$

Same as the SR-MRF (see Eq.(3)), we can also use the Algorithm 1 to obtain the ΔD^i of Eq.(4).

3. Linear interpolation

Linear interpolation algorithm is applied to obtain the inserted slice \hat{C} , given by

$$\hat{C}_{xy\hat{z}_i} = \frac{d_{\hat{z}_i, z_{j+1}} C_{\hat{x}\hat{y}z_j}}{d_{z_j, \hat{z}_i} + d_{\hat{z}_i, z_{j+1}}} + \frac{d_{z_j, \hat{z}_i} C_{\hat{x}\hat{y}z_{j+1}}}{d_{z_j, \hat{z}_i} + d_{\hat{z}_i, z_{j+1}}} \quad (5)$$

where $C_{\hat{x}\hat{y}z_j}$, $C_{\hat{x}\hat{y}z_{j+1}}$ are the voxels along the direction $D_{xy\hat{z}_i}$, and d_{z_j, \hat{z}_i} , $d_{\hat{z}_i, z_{j+1}}$ are the corresponding distances (see the dashed box of Fig.1).

IV. Experimental Results

A number of image slices are used to evaluate the performance of MR-DCI by comparing with the linear, morphology-based^[2], shape-based^[5] and registration-based^[8] methods. In MR-DCI, the iteration number $n_i = 10$, the size of the label set $n_l = 8$ (the label sets at different resolutions are not change), and the Gaussian pyramid level is set as 3, while in SR-DCI, the iteration number $n_i = 20$, the size of the label set $n_l = 24$.

Quantitative evaluation We use Q_m and Q_t as quantitative measurements, given by

$$\begin{aligned} Q_m &= \frac{1}{N_C} \sum_{x,y} (C_{xyz_i} - \hat{C}_{xyz_i})^2 \\ Q_t &= \frac{1}{N_C} \sum_{x,y} |C_{xyz_i} - \hat{C}_{xyz_i}|, \end{aligned}$$

where N_C is the voxel number.

In the first experiment¹, 22 consecutive slices are used to evaluate our method. As illustrated in Fig.2, the error measures of MR-DCI are smaller than the others. Moreover, our method is very stable. In the second experiment², we give more numerical comparisons. The average errors of all data-set are shown in Table 1. From this table, we see the two errors of MR-DCI are smaller.

Table 1. Comparison of the interpolation accuracy.
boldface: best; underline: second best

Algorithm	Linear	Morphology	Shape	DirCoherence	SR-DCI	MR-DCI
Q_m	390.5	372.9	265.2	301.6	346.1	259.8
Q_t	14.19	13.61	9.206	11.43	12.07	9.045

Qualitative evaluation The third experiment is performed on the two data sets with a translation and scaling. As shown in Fig.3, our method yields more faithful interpolation than the linear and registration-based^[8] (see voxels around the boundaries). Moreover, the object shapes and structures are both preserved better than the morphology-based^[2].

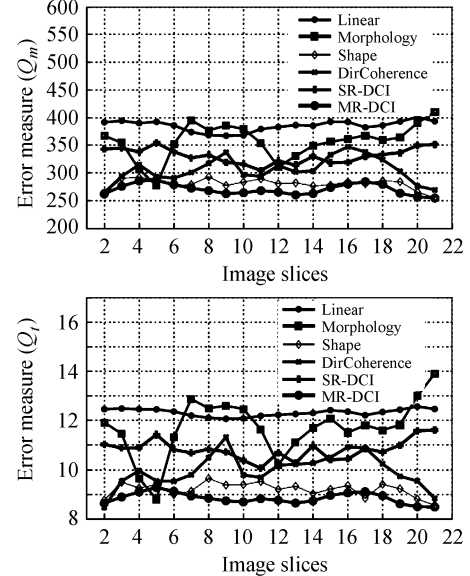


Fig. 2. Numeric comparison results. The 2 to 21 slices are selected as the reference slices (or ground truth)

The image slices are acquired by the MR technique. As shown in Fig.4, the edge features are blurred by the linear, registration-based, and morphology-based methods, while these features are well preserved by shape-based and our methods. However, the computational cost of shape-based method is very high, which will be mentioned below.

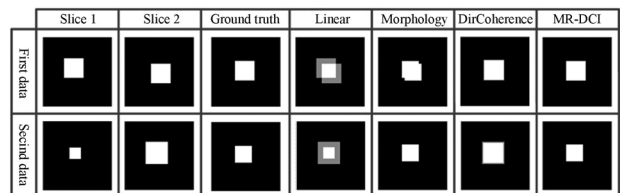


Fig. 3. Visual comparison results on two synthetic image slices

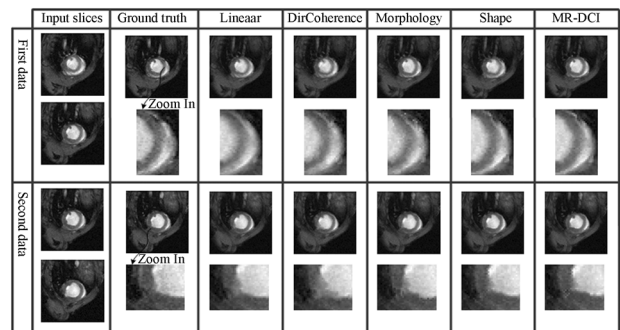


Fig. 4. Visual comparison results on real images. The local zoomed-in images are given to present the comparison in detail

Computational cost The computational cost comparisons are shown in Table 2. A standard PC with a 1.8GHz processor and 2.0GB of memory is used. All algorithms are implemented in MATLAB. The resolution of the tested slice is 256×256 . As shown in Table 2, the time consumption of MR-DCI is greatly lower than the shape-based method.

Table 2. The comparisons of the time consumption (second)

Algorithm	Linear	Morphology	Shape	Dir-Coherence	SR-DCI	MR-DCI
Time	0.0013	4.3270	199.01	21.164	80.136	12.235

Analysis of the parameters We analyze three parameters, *i.e.*, label set size n_l , Gaussian level k , and the weighting parameter λ , and the results are shown on Table 3 and Table 4. The slices tested here are the same as the second experiment of Subsection IV-1. As shown in Table 3, MR-DCI is less sensitive to n_l than k , and when $k = 3$ and $n_l = 12$, the result is best. Moreover, as can be see from this Table 4, our method is to some extent stable to the weighting parameter λ .

Table 3. Comparisons of Q_m and Q_t with different parameters. boldface: best

Q_m	$n_l = 4$	$n_l = 8$	$n_l = 12$	$n_l = 24$
$k = 1$	427.8	484.2	452.7	346.1
$k = 2$	321.5	299.6	287.2	279.0
$k = 3$	281.0	259.8	250.3	271.5
$k = 4$	268.2	264.6	301.9	352.1
$k = 5$	302.8	355.1	419.4	482.5
Q_t	$n_l = 4$	$n_l = 8$	$n_l = 12$	$n_l = 24$
$k = 1$	16.48	16.87	15.25	12.07
$k = 2$	11.21	10.43	10.00	9.722
$k = 3$	9.789	9.045	8.721	9.458
$k = 4$	9.348	9.215	10.52	12.26
$k = 5$	10.54	12.37	14.61	16.81

Table 4. Comparisons of Q_m and Q_t with different λ ($n_l = 8$ and $k = 3$). boldface: best

	$\lambda = 10^{-2}$	$\lambda = 10^{-1}$	$\lambda = 1$	$\lambda = 10$	$\lambda = 10^2$
Q_m	272.1	264.5	259.8	262.4	266.8
Q_t	9.427	9.210	9.045	9.106	9.216

V. Conclusions

A novel MR-DCI method is presented in this paper. The proposed scheme has the following advantages. First, performing directly on the gray-scale image slices can avoid the preprocessing as required in morphology-based. Hence, our method can be applied to more general interpolation cases. Second, the rotation-invariant template is used as the local feature descriptor to overcome high computational costs in the shape-based and registration-based methods. Third, for each voxel, we calculate its direction other than intensity. Meanwhile, multi-resolution scheme is adopted in this work. These can further lower computational cost as well as enhance interpolation accuracy. In the future, we will adopt more sophisticated interpolation algorithm, such as spline, to further enhance our method.

References

- [1] G.J. Grevera and J.K. Udupa, "An objective comparison of 3-D image interpolation methods", *IEEE Transactions on Medical Imaging*, Vol.17, No.4, pp.642–652, 1998.

- [2] T.Y. Lee and W.H. Wang, "Morphology-based three-dimensional interpolation", *IEEE Transactions on Medical Imaging*, Vol.19, No.7, pp.711–721, 2000.
- [3] A.B. Albu, T. Beugeling and D. Laurendeau, "A morphology-based approach for interslice interpolation of anatomical slices from volumetric images", *IEEE Transactions on Medical Imaging*, Vol.55, No.8, pp.2022–2038, 2008.
- [4] X. Yanlei, Z. Jiayin, L. Min and Z. Tingting, "The interpolation arithmetic study of medical image based on the order morphology", *Acta Electronica Sinica*, Vol.38, No.1, pp.82–84, 2010. (in Chinese)
- [5] G.J. Grevera and J.K. Udupa, "Shape-based interpolation of multidimensional grey-level images", *IEEE Transactions on Medical Imaging*, Vol.15, No.6, pp.881–892, 1996.
- [6] G.P. Penney, J.A. Schnabel, D. Rueckert, M.A. Viergever and W.J. Niessen, "Registration-based interpolation", *IEEE Transactions on Medical Imaging*, Vol.23, No.7, pp.922–926, 2004.
- [7] D. Frakes, L. Dasi, K. Pekkan, H. Kitajima, K. Sundareswaran, A. Yoganathan and M. Smith, "A new method for registration-based medical image interpolation", *IEEE Transactions on Medical Imaging*, Vol.27, No.3, pp.370–377, 2008.
- [8] Y. Wang, J. Zhang, Z. Zhang and B. Guo, "Directional coherence interpolation for three-dimensional gray-level images", *International Journal of Image and Graphics*, Vol.4, No.4, pp.535–561, 2004.
- [9] T. Xiaoying, W. Liye and L. Weifeng, "A comprehensive interpolation for medical slices based on combination of linear and matching interpolation", *Chinese Journal of Electronics*, Vol.20, No.1, pp.82–84, 2011.
- [10] S.Z. Li, *Markov Random Field Modeling in Image Analysis*, Secaucus, NJ, USA: Springer-Verlag New York, Inc., 2001.



WANG Lingfeng received B.S. degree in computer science from Wuhan University, Wuhan, China, in 2007. He is currently pursuing the Ph.D. degree in Institute of Automation, Chinese Academy of Sciences. His research interests include computer vision and image processing. (Email: lfwang@nlpr.ia.ac.cn)



YU Zeyun received B.S. degree in mathematics from Peking University (China) in 1996 and the M.S. degree in pattern recognition and machine intelligence from Chinese Academy of Sciences (China) in 1999. He received the Ph.D. degree in computer science from The University of Texas at Austin in 2006 and then worked as a postdoctoral scholar at Department of Mathematics, University of California-San Diego. Since August 2008, he has been an assistant professor in Department of Computer Science, University of Wisconsin-Milwaukee. His research interests span from algorithms in image analysis, geometric processing, scientific computing and visualization, to applications in structural and functional modeling of biomedical systems.



PAN Chunhong received B.S. degree in automatic control from Tsinghua University, Beijing, China, in 1987, M.S. degree from Shanghai Institute of Optics and Fine Mechanics, Chinese Academy of Sciences, China, in 1990, and Ph.D. degree in pattern recognition and intelligent system from Institute of Automation, Chinese Academy of Sciences, Beijing, in 2000. He is currently a professor with the National Laboratory of Pattern Recognition of Institute of Automation, Chinese Academy of Sciences. His research interests include computer vision, image processing, computer graphics, and remote sensing.